Internal resonance responses of rectangular cross-ply composite plates with graphene skins

Xiangying Guo[a], Pan Jiang[a], Wenhan Yan[a], Siu-Kai Lai[b,c,*], Wei Zhang[a]

[a] *Beijing Key Laboratory of Nonlinear Vibrations and Strength of Mechanical Structures, College of Mechanical Engineering, Beijing University of Technology, Beijing, 100124, P.R. China*

[b] *Department of Civil and Environmental Engineering, The Hong Kong Polytechnic University, Hung Hom, Kowloon, Hong Kong, P.R. China*

[c] *The Hong Kong Polytechnic University Shenzhen Research Institute, Shenzhen, P.R. China*

Abstract: This paper presents an investigation on the nonlinear dynamic behavior of three-phase composite plates made of cross-ply macro fiber composites (MFC) in the polymer with graphene (GP) skins, which are uniformly dispersed at the top and bottom surfaces of the plates. According to the mixture rules for multi-components of composite materials, the constitutive laws for MFC-GP composite materials can be obtained. A four-edge simply-supported rectangular plate model subjected to a transversal excitation in thermal environments is considered. The governing equations are formulated by using the first-order shear deformation theory, von Kármán geometrical kinematics and Hamilton's principle. Then, the Galerkin approach is used to discretize the governing equations for analysis. The vibration frequencies of MFC-GP composite plates with different modes are presented and the case of 1:2 internal resonance is selected to be investigated here. Different coupled forms (i.e., uncoupled, weakly coupled and strongly coupled cases) of two vibration modes are presented. In addition, the influences of various parameters, including volume fraction of graphene, applied voltage, temperature effect and external excitation, on the nonlinear dynamic characteristics of MFC-GP composite plates are also examined.

Keywords: MFC-GP composite plate; Graphene; Nonlinear vibration; Internal resonance

[*]Corresponding author. Tel.: (852) 2766 6060; Fax: (852) 2334 6389. *E-mail address:* sk.lai@polyu.edu.hk

1. Introduction

Graphene is the first isolated 2D material with a hexagonal lattice of sp^2 hybridized carbon atoms [1], the intrinsic nature is a semi-metal with small overlap between the valence and the conduction bands. Such a material possesses high thermal conductivity and remarkable mechanical properties. Due to its superiority, a lamination of smart materials (e.g., piezoelectric and functionally graded materials) with graphene as composite structures can enhance the versatility in a wide range of areas. Graphene composite materials have been recently used in various engineering structures, e.g., energy storage materials, biological materials and conductive ink [2]. Nevertheless, there are still significant challenges ahead of exploring the potential applications of graphene composite materials, as it is highly desired to understand the dynamic behaviour of graphene composite materials under different conditions in real-life applications.

In the literature, many research studies reported the nonlinear dynamical behaviour of various composite structures. For example, Zhang et al. [3] investigated the nonlinear vibration and chaotic dynamics of orthotropic functionally graded material rectangular plates under a combination of transverse and in-plane excitations. The considered resonant case is 1:2:4 internal resonance, and the principal parametric resonance-subharmonic resonance is of order 1/2. Ansari et al. [4] compared the linear resonant frequencies of graphene sheets via the nonlocal elasticity theory and molecular dynamics simulations. Xu et al. [5] enriched the understanding of electromechanical properties of graphene and its potential applications in the field of nano-electro-mechanical systems and flexible electronics. In addition, Li and Wang [6] presented an analytical method to calculate nonlinear frequency shifts of graphene-elastic-piezoelectric laminated films that can be acted as a resonant mass detector. Zhu et al. [7] studied the nonlinear dynamics and bifurcation of Al-doped graphene. Shen et al. [8-9] further investigated the nonlinear vibration analysis of graphene-reinforced composite laminated beams and panels resting on an elastic foundation in thermal environments. More recently, Guo et al. [10] investigated the nonlinear dynamical behaviour of cantilevered composite plates made of graphene with a macro fiber composite in the polymer.

On the dynamical stability and vibration modes of composite structures, Wu et al. [11] studied the nonlinear normal modes of physical systems by introducing an undivided even-dimensional invariant manifold. Li et al. [12] applied the method of multiple scales to construct the nonlinear normal modes of two beams connected by a coupling spring having cubic nonlinearity. Lacarbonara and his co-workers [13-14] considered the resonant non-linear normal

modes of weakly nonlinear one-dimensional continuous systems with quadratic and cubic geometric nonlinearities. Sayed and Mousa [15] investigated the influence of the quadratic and cubic nonlinear terms on the dynamic characteristics of angle-ply composite laminated rectangular plates subject to parametric and external excitations. Furthermore, the softening and hardening behavior of initially curved graphene sheets was studied using the nonlocal continuum theory, it was found that the bending stiffness of initially curved graphene sheets is curvature dependent [16]. Kwon et al. [17-18] discussed the vibration characteristics of graphene-based resonators by molecular dynamics simulations. Additionally, Mousa et al. [19] also analyzed the stability of simply supported laminated composite piezoelectric rectangular plates under combined excitations. Mao et al. [20] investigated that linear and nonlinear free and forced vibrations of graphene reinforced piezoelectric composite plate under external voltage excitation. Lai and Zhang [21] presented the linear vibration and buckling analysis of orthotropic plates with crack defects in thermal environments.

On the other hand, the thermal transport properties of graphene composites are also another key topic to explore its potential applications. Ji et al. [22] embedded continuous ultrathin-graphite foams in phase change materials to enhance the thermal conductivity for thermal energy storage. Ma et al. [23] systematically investigated the temperature dependent transport and thermoelectric properties of graphene fibers, including thermal conductivity, electrical conductivity and Seebeck coefficient. Some research studies also discussed the thermal conductive mechanisms in the interface of graphene-polymer composites [24-25]. In addition to these studies, Zhang et al.[26] focused on modulating the thermal transport across the graphenepolymer interface by means of a non-covalent functionalization technique. Yang et al. [27] analyzed the thermo-elastic bending behavior of functionally graded polymer nanocomposite rectangular plates reinforced with graphene nanoplatelets. Phiri et al. [28] used graphene, graphene oxide and reduced graphene oxide as reinforcement functional fillers for the fabrication of multifunctional MFC nanocomposites using a simple aqueous dispersion based on a mixing method. Shahrjerdi and Yavari [29] further investigated the temperature-dependent vibration for functionally graded nanocomposite beams that are reinforced by graphene.

However, there are still few studies devoted to conduct a parametric analysis for the nonlinear dynamic behavior of cross-ply MFC-GP composite plates in thermal environments. In this paper, analytical solutions for the dynamical behavior of such composite plates are derived in accordance with the Galerkin procedure and the multi-scale method. A numerical

approach is then applied to investigate the internal resonance response of MFC-GP composite plates. Effects of various parameters, including volume fraction of graphene, applied voltage, temperature difference and external excitation, on the nonlinear dynamic characteristics of MFC-GP composite plates is also examined. Finally, the nonlinear characteristics of the system are revealed and discussed.

2. Constitutive relations of the MFC-GP material

Consider a three-phase composite material, which contains MFC sheets in the matrix by orthogonal laying and graphene skins as shown in Fig. 1 [10]. The constitutive relations for MFC-GP materials can be obtained by two steps. The first one is to construct the relations of the MFC material, and the second one is to consider the composite with graphene skins.

According to the superposition principle [30], the Young's modulus of the three-phase composite can be expressed as

$$E_c = E_g a_g + \left(1-a_g\right)\left(E_p a_p + \left(1-a_p\right)E_m\right) \tag{1}$$

where E_g , E_p and E_m are the Young's modulus of the graphene, MFC and matrix, respectively. a_g and a_p are the volume fractions of the graphene and MFC, respectively.

Meanwhile, the Poisson's ratio (υ), thermal expansion coefficient (α) and the intensity of electric fields of composite materials (E_3) can be obtained by the rule of mixture as follows [8, 27, 31]:

$$\upsilon = \upsilon_g a_g + \left(1-a_g\right)\left(\upsilon_p a_p + \left(1-a_p\right)\upsilon_m\right) \tag{2}$$

$$\alpha = \alpha_g a_g + \left(1-a_g\right)\left(\alpha_p a_p + \left(1-a_p\right)\alpha_m\right) \tag{3}$$

$$E_3 = \frac{U}{t_g} a_g + \left(1-a_g\right)\frac{U}{t_p} a_p \tag{4}$$

where U is an external voltage, t_g and t_p are the thickness of the graphene and MFC, respectively.

The piezoelectric-strain parameters for composite materials d_{3i} (i = 1, 2) can be expressed

$$d_{3i} = \frac{M_i}{N_i} \qquad \left(i = 1, 2\right) \tag{5}$$

where M_i and N_i are related to the piezoelectric constant (g_i), volume fractions (a_g, a_p)

and flexibility coefficient (s_i). The analytical expressions of M_i and N_i are given in Appendix.

According to the properties of composite materials, the constitutive laws for the MFC-GP composite material are

$$\begin{Bmatrix} \sigma_1 \\ \sigma_2 \\ \sigma_4 \\ \sigma_5 \\ \sigma_6 \end{Bmatrix} = \begin{bmatrix} Q_{11} & Q_{12} & 0 & 0 & 0 \\ Q_{21} & Q_{22} & 0 & 0 & 0 \\ 0 & 0 & Q_{44} & 0 & 0 \\ 0 & 0 & 0 & Q_{55} & 0 \\ 0 & 0 & 0 & 0 & Q_{66} \end{bmatrix} \left\{ \begin{bmatrix} \varepsilon_{xx} \\ \varepsilon_{yy} \\ 0 \\ 0 \\ \gamma_{xy} \end{bmatrix} - \begin{bmatrix} \alpha \\ \alpha \\ 0 \\ 0 \\ 0 \end{bmatrix} \Delta T - \begin{bmatrix} d_{31} \\ d_{32} \\ 0 \\ 0 \\ 0 \end{bmatrix} E_3 \right\} \tag{6}$$

where E_3 denotes the intensity of electric fields of composite materials and ΔT is temperature difference between the upper and lower surfaces of the composite material plate. The unit form of the elements Q_{ij} can be written as $Q_{11}=\frac{E_c}{1-\upsilon^2}=Q_{22}$, $Q_{12}=\frac{\upsilon E_c}{1-\upsilon^2}=Q_{21}$ and $Q_{44}=Q_{55}=Q_{66}=\frac{E_c}{2(1-\upsilon)}$.

3. Theoretical modelling

Consider a simply-supported MFC-GP plate with length a , width b and uniform thickness h. The plate is made of cross-ply MFC in the polymer with graphene skins, and it is subject to a transversal excitation, as shown in Fig. 2. The displacement fields of an arbitrary point within the plate in the *x, y* and *z* directions are u , v and w, respectively.

According to the first-order shear deformation theory [32], the displacement fields of the MFC-GP plate can be expressed in the following form

$$u(x,y,z,t)=u_0(x,y,t)-z\phi_x(x,y,t) \tag{7a}$$

$$v(x,y,z,t)=v_0(x,y,t)-z\phi_y(x,y,t) \tag{7b}$$

$$w(x,y,z,t)=w_0(x,y,t) \tag{7c}$$

where , ϕ_x,ϕ_y is the rotation angle of the normal line of the plate to the X axis and the y axis respectively , u_0 , v_0 and w_0 are the displacements of the neutral surface of the plate along the *x, y* and *z* directions.

From the von Kármán-type theory [33], the relations between the strain and the displacement are obtained as follows

$$\varepsilon_{xx} = \frac{\partial u_0}{\partial x} + \frac{1}{2}\left(\frac{\partial w_0}{\partial x}\right)^2 - z\frac{\partial^2 w_0}{\partial x^2} \tag{8a}$$

$$\varepsilon_{yy} = \frac{\partial v_0}{\partial y} + \frac{1}{2}\left(\frac{\partial w_0}{\partial y}\right)^2 - z\frac{\partial^2 w_0}{\partial y^2} \tag{8b}$$

$$\gamma_{xy} = \frac{\partial u_0}{\partial y} + \frac{\partial v_0}{\partial x} + \frac{\partial w_0}{\partial x}\frac{\partial w_0}{\partial y} - 2z\frac{\partial^2 w_0}{\partial x \partial y} \tag{8c}$$

The nonlinear governing equations of motion for the MFC-GP plate can be derived by the Hamilton's principle as follows

$$N_{xx,x} + N_{xy,y} = I_0\frac{\partial^2 u_0}{\partial t^2} - I_1\frac{\partial^3 w_0}{\partial x \partial t^2} \tag{9a}$$

$$N_{xy,x} + N_{yy,y} = I_0\frac{\partial^2 v_0}{\partial t^2} - I_1\frac{\partial^3 w_0}{\partial y \partial t^2} \tag{9b}$$

$$N_{xx,x}\frac{\partial w_0}{\partial x} + N_{xx}\frac{\partial^2 w_0}{\partial x^2} + N_{xy,x}\frac{\partial w_0}{\partial y} + 2N_{xy}\frac{\partial^2 w_0}{\partial x \partial y} + N_{xy,y}\frac{\partial w_0}{\partial x} + N_{yy,y}\frac{\partial w_0}{\partial y} + N_{yy}\frac{\partial^2 w_0}{\partial y^2} +$$

$$\left(M_{xx,x} + M_{xy,y}\right)_{,x} + \left(M_{xy,x} + M_{yy,y}\right)_{,y} + F\cos(\Omega t) - r\frac{\partial w_0}{\partial t} = I_0\frac{\partial^2 w_0}{\partial t^2} + I_1\left(\frac{\partial^3 u_0}{\partial x \partial t^2} + \frac{\partial^3 v_0}{\partial y \partial t^2}\right)$$

$$-I_2\left(\frac{\partial^4 w_0}{\partial x^2 \partial t^2} + \frac{\partial^4 w_0}{\partial y^2 \partial t^2}\right) \tag{9c}$$

in which

$$\begin{Bmatrix} N_{xx} \\ N_{yy} \\ N_{xy} \end{Bmatrix} = \begin{bmatrix} A_{11} & A_{12} & 0 \\ A_{21} & A_{22} & 0 \\ 0 & 0 & A_{66} \end{bmatrix}\begin{bmatrix} \varepsilon_{xx}^0 \\ \varepsilon_{yy}^0 \\ \gamma_{xy}^0 \end{bmatrix} + \begin{Bmatrix} N_{t1} \\ N_{t2} \\ N_{t12} \end{Bmatrix} + \begin{Bmatrix} N_{e1} \\ N_{e2} \\ N_{e12} \end{Bmatrix} \tag{10a}$$

$$\begin{Bmatrix} M_{xx} \\ M_{yy} \\ M_{xy} \end{Bmatrix} = \begin{bmatrix} D_{11} & D_{12} & 0 \\ D_{21} & D_{22} & 0 \\ 0 & 0 & D_{66} \end{bmatrix}\begin{bmatrix} \varepsilon_{xx}^1 \\ \varepsilon_{yy}^1 \\ \gamma_{xy}^1 \end{bmatrix} + \begin{Bmatrix} M_{t1} \\ M_{t2} \\ M_{t12} \end{Bmatrix} + \begin{Bmatrix} M_{e1} \\ M_{e2} \\ M_{e12} \end{Bmatrix} \tag{10b}$$

$$\left(A_{ij}, D_{ij}\right) = \int_{-\frac{h}{2}}^{\frac{h}{2}} Q_{ij}\left(1, z^2\right)dz \qquad I_0 = \int_{-\frac{h}{2}}^{\frac{h}{2}} \rho dz \qquad I_1 = \int_{-\frac{h}{2}}^{\frac{h}{2}} \rho z dz \qquad I_2 = \int_{-\frac{h}{2}}^{\frac{h}{2}} \rho z^2 dz \tag{11}$$

The boundary conditions of a four-edge simply supported plate are given by

$$x = 0, a: \quad w = 0, \quad \frac{\partial^2 w}{\partial x^2} = 0 \tag{12a}$$

$$y = 0, b: \quad w = 0, \quad \frac{\partial^2 w}{\partial y^2} = 0 \tag{12b}$$

The dimensionless variables are then introduced as follows

$$\overline{w} = \frac{w_0}{h}, \ \overline{u} = \frac{u_0}{a}, \ \overline{v} = \frac{v_0}{b}, \ \overline{F} = \frac{(ab)^{\frac{7}{2}}}{Eh^7} F, \ \overline{x} = \frac{x}{a}, \ \overline{y} = \frac{y}{b}$$

$$\overline{A}_{ij} = \frac{(ab)^{\frac{1}{2}}}{Eh^2} A_{ij}, \ \overline{D}_{ij} = \frac{(ab)^{\frac{1}{2}}}{Eh^4} D_{ij}, \ \overline{I}_{ij} = \frac{1}{(ab)^{\frac{i+1}{2}} \rho} I_{ij}, \ \overline{t} = \pi^2 \left(\frac{E}{ab\rho} \right)^{\frac{1}{2}} t \tag{13}$$

For convenience and brevity, bars above the symbols in Eq. (13) are omitted in the subsequent analysis.

Based on the boundary conditions, the normalized transverse displacement (w) can be expressed in the following form

$$w(x, y, t) = \sum_{m=1}^{\infty} \sum_{n=1}^{\infty} w_{mn}(t) \sin \frac{m\pi x}{a} \sin \frac{n\pi y}{b} \tag{14}$$

In the present case, natural frequencies of the system can be calculated using the nonlinear dynamical theory. The ordinary differential equation is obtained as follows

$$\ddot{w}_i + \lambda_i \dot{w}_i + \omega_i^2 w_i + \left(t_i \cos(\Omega_i t) + p_i \cos(\Omega_i t) \right) w_i + \xi_{i1} w_i^3 = \xi_{i2} F_i \cos(\Omega_i t) \tag{15}$$

where λ_i is the damping coefficient, ζ_{i1} and ζ_{i2} are the cubic nonlinear terms and ω_i is the natural frequency of a linear system in Eq. (15). t_i and p_i represent the thermal and piezo-electrical parameters of the system, respectively.

By omitting the nonlinear and damping terms in Eq. (15), we have

$$L_1 = w_i \qquad L_2 = \dot{w}_i \tag{16}$$

Then, Eq. (15) is re-written in the following forms

$$\frac{\partial L_1}{\partial t} = L_2 \tag{17a}$$

$$\frac{\partial L_2}{\partial t} = -\omega_i^2 L_1 - \left(t_i \cos(\Omega_i t) + p_i \cos(\Omega_i t) \right) L_1 + \xi_{i2} F_i \cos(\Omega_i t) \tag{17b}$$

Meanwhile, we introduce a state-space representation. Therefore, Eq. (17) can be expressed in the following matrix

$$\begin{bmatrix} \dot{L}_1 \\ \dot{L}_2 \end{bmatrix} = \begin{bmatrix} 0 & 1 \\ \Gamma & 0 \end{bmatrix} \begin{bmatrix} L_1 \\ L_2 \end{bmatrix} + \begin{bmatrix} 0 \\ R \end{bmatrix} \tag{18}$$

where

$$\Gamma = -\omega_i^2 - t_i \cos(\Omega_i t) - p_i \cos(\Omega_i t),\ R = \xi_{i2} F_i \cos(\Omega_i t) \tag{19}$$

By introducing trivial solutions, the stability of the solution of any linear system can be reduced to the stability of the zero solution of the corresponding linear homogeneous system. Let J be a 2×2 Jacobian matrix of the vector field L_j at a point.

$$J = \begin{bmatrix} 0 & 1 \\ \Gamma & 0 \end{bmatrix} \tag{20}$$

If all eigenvalues of *J* have strictly negative real parts, the solution is stable and the imaginary parts are the natural frequencies of the system. If one of the eigenvalues of *J* is positive than zero, the system is unstable and the imaginary parts cannot be used to calculated the natural frequencies of the system. The physical parameters of the MFC-GP plate in Table 1 are considered. The geometrical parameters of the plate are chosen as $a = 1.5$ m, $b = 1$ m, $h = 0.002$ m. Besides, we assume that the extra coupled fields can satisfy $\Delta T = 500°C$ and $U = 1kV$. Hence, the natural frequencies of the plate structure can be obtained through the negative eigenvalues of *J* in Table 2.

Based on the above analysis in Table 2, we observe that the case of 1:2 internal resonance appears between the vibration modes *m*=*n*=1 and *m*=3, *n*=1. To consider complex dynamical behavior of the MFC-GP composite plate, the normalized transverse displacement *w* is now changed to

$$w(x, y, t) = w_1(t) \sin\left(\frac{\pi x}{a}\right) \sin\left(\frac{\pi y}{b}\right) + w_2(t) \sin\left(\frac{3\pi x}{a}\right) \sin\left(\frac{\pi y}{b}\right) \tag{21a}$$

Meanwhile, piezoelectrical and temperature forces are also discretized as follows

$$N_{ei} = N_{ei1}(t) \cos(\Omega_2 t) \sin\left(\frac{\pi x}{2a}\right) \cos\left(\frac{\pi y}{b}\right) + N_{ei2}(t) \cos(\Omega_2 t) \sin\left(\frac{3\pi x}{2a}\right) \cos\left(\frac{2\pi y}{b}\right), i = 1,2 \tag{21b}$$

$$N_{tj} = N_{tj1}(t) \cos(\Omega_3 t) \sin\left(\frac{\pi x}{2a}\right) \cos\left(\frac{\pi y}{b}\right) + N_{tj2}(t) \cos(\Omega_3 t) \sin\left(\frac{3\pi x}{2a}\right) \cos\left(\frac{2\pi y}{b}\right), j = 1,2 \tag{21c}$$

Then, we apply the Galerkin procedure to obtain a set of second-order ordinary differential equations. Substituting the above physical parameters into the equations and ignoring the higher-order terms, the governing equations for the transverse motion of the MFC-GP plate are formulated as

$$\ddot{w}_1 + \mu_1 \dot{w}_1 + k_{11} w_1^3 + k_{12} w_2^3 + k_{13} w_1^2 w_2 + k_{14} w_1 w_2^2 + \omega_1^2 w_1 + \left(p_{11} \cos\left(\Omega_2 t\right) + t_{11} \cos\left(\Omega_3 t\right) \right) w_1 + \left(p_{12} \cos\left(\Omega_2 t\right) + t_{12} \cos\left(\Omega_3 t\right) \right) w_2 = k_{15} F_1 \cos\left(\Omega_1 t\right) \tag{22a}$$

$$\ddot{w}_2 + \mu_2 \dot{w}_2 + k_{21} w_1^3 + k_{22} w_2^3 + k_{23} w_1^2 w_2 + k_{24} w_1 w_2^2 + \omega_2^2 w_2 + \left(p_{21} \cos\left(\Omega_2 t\right) + t_{21} \cos\left(\Omega_3 t\right) \right) w_1 + \left(p_{22} \cos\left(\Omega_2 t\right) + t_{22} \cos\left(\Omega_3 t\right) \right) w_2 = k_{25} F_2 \cos\left(\Omega_1 t\right) \tag{22b}$$

where the coefficients k_{ij} (i =1, 2; j =1–4) are the parameters of the cubic nonlinear terms and k_{ij} (i =1, 2; j = 5) are the parameters of the forcing terms. t_{ij} and p_{ij} (i=1, 2; j=1, 2) represent the thermal and piezo-electrical parameters of the system, respectively.

4. Perturbation analysis

In this section, a perturbation analysis for the ordinary differential equations using the multi-scale method is performed. The solution forms of Eq. (22) are written as [34]

$$w_1 = w_{10}\left(T_0, T_1\right) + \varepsilon w_{11}\left(T_0, T_1\right) + \ldots \tag{23a}$$

$$w_2 = w_{20}\left(T_0, T_1\right) + \varepsilon w_{21}\left(T_0, T_1\right) + \ldots \tag{23b}$$

where $T_0 = t$ and $T_1 = \varepsilon t$.

Consider the case of 1:2 internal resonance, we assume

$$\omega_1 = \frac{1}{2}\Omega_1 - \varepsilon\sigma_1, \quad \omega_2 = \Omega_1 - \varepsilon\sigma_2 \quad , \ \Omega_1 = \Omega_2 = \Omega_3 = 1 \tag{24}$$

where ω_1 and ω_2 are the first and second order natural frequencies, respectively. σ_1 and σ_2 are two detuning parameters.

In terms of a polar form, the averaged equations are obtained after the perturbation analysis as

$$\dot{a}_1 = -\frac{1}{2}\mu_1 a_1 + \frac{1}{2}\left(t_{11} + p_{11}\right) a_1 \sin\left(2\beta_1\right) \tag{25a}$$

$$a_1\dot{\beta}_1 = \frac{3}{4}k_{11}a_1^3 + \frac{1}{2}k_{14}a_1 a_2^2 - \sigma_1 a_1 + \frac{1}{2}\left(t_{11} + p_{11}\right) a_1 \cos\left(2\beta_1\right) \tag{25b}$$

$$\dot{a}_2 = -\frac{1}{2}\mu_2 a_2 - \frac{k_{25}F}{2}\sin\left(\beta_2\right) \tag{25c}$$

$$a_2\dot{\beta}_2 = \frac{3}{8}k_{22}a_2^3 + \frac{1}{4}k_{23}a_1^2 a_2 - \sigma_2 a_2 - \frac{k_{25}F}{2}\cos\left(\beta_2\right) \tag{25d}$$

where a_i and β_i (i=1, 2) represent the amplitudes and phases of the system.

To analyze the energy transformation between two coupled modes, the relationship of the

nonlinear terms in two modes are considered here. They are uncoupled, weekly coupled and strongly coupled cases. We assume that the right-hand side of Eq. (25) is equal to zero to eliminate the terms $2\beta_1$ and β_2 by using the trigonometric relations. The frequency-response functions can then be obtained as

$$\left(-\frac{1}{2}\mu_1 a_1\right)^2+\left(\frac{3}{4}k_{11}a_1^3+\frac{1}{2}k_{14}a_1a_2^2-\sigma_1 a_1\right)^2=\frac{1}{4}\left(t_{11}+p_{11}\right)^2 a_1^2 \tag{26a}$$

$$\left(-\frac{1}{2}\mu_2 a_2\right)^2+\left(\frac{3}{8}k_{22}a_2^3+\frac{1}{4}k_{23}a_1^2a_2-\sigma_2 a_2\right)^2=\frac{k_{25}^2F^2}{4} \tag{26b}$$

Setting $a_2 = 0$ in Eq. (26a) and $a_1 = 0$ in Eq. (26b), this is the uncoupled case between two modes of the system. The frequency-response functions of the two modes in the system are

$$\left(-\frac{1}{2}\mu_1 a_1\right)^2+\left(\frac{3}{4}k_{11}a_1^3-\sigma_1 a_1\right)^2=\frac{1}{4}\left(t_{11}+p_{11}\right)^2 a_1^2 \tag{27a}$$

$$\left(-\frac{1}{2}\mu_2 a_2\right)^2+\left(\frac{3}{8}k_{22}a_2^3-\sigma_2 a_2\right)^2=\frac{k_{25}^2F^2}{4} \tag{27b}$$

Various frequency-response curves of the system can be obtained by adjusting different parameters of the system, including graphene volume fraction, voltage, temperature and external excitation force, as presented Figs 3-7. Figures 3 and 4 show the effect of volume fraction on the first- and second-order modes, in which both frequency-response curves bend to the right side. It refers to the structure with the hardening spring characteristic, which becomes stronger with increasing the volume fraction of GP. Meanwhile, the amplitude of the structure decreased with the varies of the volume fraction of GP. In Figs. 5 and 6, the resonance region is bigger with increasing either temperature or external excitation. However, the effect of voltage changes on the frequency-response curve is not pronounced as shown in Fig. 7. In the literature, some research works (e.g. Ref. 28) have discussed the thermal stability of graphene-based composite materials in the temperature pattern between 25–800°C. Moreover, Wu et al.[35] studied the thermal stability of epoxy resins at about 350–500°C. A high-temperature resistant glue for composite materials is considered here, which can work well in thermal fields. Hence, the structure studied here can be subject to the temperature difference at $\Delta T = 500°C$.

The weakly coupled case of two modes is also studied and compared with the uncouple

one. Consider a_2=1 in Eq. (26a) and a_1=1 in Eq. (26b). The frequency-response functions for the weakly coupled case of two modes in the system are obtained as

$$\left(-\frac{1}{2}\mu_1 a_1\right)^2+\left(\frac{3}{4}k_{11}a_1^3+\frac{1}{2}k_{14}a_1-\sigma_1 a_1\right)^2=\frac{1}{4}\left(t_{11}+p_{11}\right)^2 a_1^2 \tag{28a}$$

$$\left(-\frac{1}{2}\mu_2 a_2\right)^2+\left(\frac{3}{8}k_{22}a_2^3+\frac{1}{4}k_{23}a_2-\sigma_2 a_2\right)^2=\frac{k_{25}^2F^2}{4} \tag{28b}$$

Figures 8-12 show that the plate has the hardening spring characteristic in the first- and second-order modes, and the nonlinear behaviour of the structure does not change with the weakly coupling effect. Only the frequency response curves move some distance to the right, this indicates that the resonant frequencies of the system are increased. The effect of voltage changes on the frequency-response curves is still not obvious as shown in Fig.12.

The last case to investigate is the strongly coupled case of two modes for the composite plate. Solving Eq. (26a) yields,

$$a_1^2=\frac{1}{3k_{11}}\left(4\sigma_1-2k_{14}a_2^2+2\Theta\right) \tag{29a}$$

$$a_2^2=\frac{1}{k_{14}}\left(2\sigma_1-\frac{3k_{11}}{2}a_1^2+\Theta\right) \tag{29b}$$

where $\Theta=\pm\sqrt{\left(t_{11}+p_{11}\right)^2-\mu_1^2}$.

Substituting Eq. (29) into Eq. (26b), the frequency-response functions of the strongly coupled case are derived as

$$\left(-\frac{1}{2}\mu_2\right)^2+\left(\frac{3}{8}k_{22}\left(\frac{1}{k_{14}}\left(2\sigma_1-\frac{3k_{11}}{2}a_1^2+\Theta\right)\right)+\frac{1}{4}k_{23}a_1^2-\sigma_2\right)^2=\frac{k_{25}^2F^2}{4\left(\frac{1}{k_{14}}\left(2\sigma_1-\frac{3k_{11}}{2}a_1^2+\Theta\right)\right)} \tag{30a}$$

$$\left(-\frac{1}{2}\mu_2 a_2\right)^2+\left(\frac{3}{8}k_{22}a_2^3+\frac{1}{4}k_{23}\left(\frac{1}{3k_{11}}\left(4\sigma_1-2k_{14}a_2^2+2\Theta\right)\right)a_2-\sigma_2 a_2\right)^2=\frac{k_{25}^2F^2}{4} \tag{30b}$$

It is noted that the positive or negative signs in Θ do not affect the analysis results [33], only one situation is thus considered here. From the above resonance relationships, $\left(\sigma_2-\sigma_1\right)\varepsilon=\omega_2-2\omega_1$ and $\left(\sigma_2-\sigma_1\right)\varepsilon=0$, it can be obtained as $\sigma_1=\sigma_2$.

For the strongly coupled case of two modes, various frequency-response curves are plotted. Fig. 13 shows that the system still has the hardening spring characteristic in the first-order mode and the properties become prominent when increasing the volume fraction of graphene among all three cases. Moreover, the second-order mode of the system shows the

soft spring characteristic and becomes stronger when increasing the volume fraction of graphene in Fig. 14. The reason for this phenomenon is that the second-order nonlinear terms change with the volume fraction of graphene, which have strong influence on the nonlinear spring characteristic. Additionally, Figs.15 and 16 illustrate the resonance frequency in the first- and second-order modes decrease when increasing temperature. The resonance regions of the first- and second- order increases with the increase of external excitation are presented in Figs.17 and 18. The effect of voltage change on the frequency-response curves is still not obvious as shown in Figs. 19 and 20.

Based on the above results, a comparison among three different cases is summarized in Table 3. The nonlinear characteristics of the system are similar in the uncoupled and weakly coupled cases, while it is different from the strongly coupled one under 1:2 internal resonance.

5. Conclusions

The nonlinear coupled problem of rectangular cross-ply MFC-GP plates with 1:2 inner resonance subjected to a transversal excitation in thermal environments is investigated. The governing equations of MFC-GP plates are formulated for the stability analysis. Natural frequencies of the plates are calculated and the case of 1:2 internal resonance is studied. Numerical simulation is conducted to study the effects of different parameters on the nonlinear characteristics of the MFC-GP plate. The results show that the structural properties of two modes in the weakly coupled case are consistent, while the characteristics of the first-order mode in the strongly coupled case are very different with that of the second-order mode. It is also found that the nonlinear resonance effect becomes dominant with the increase of graphene volume fraction, temperature and transversal excitation under different coupled modes. However, the effect of external voltage on these coupled and uncoupled cases are not obvious, this may be due to the simple supported boundary conditions.

In this study, we only consider the nonlinear dynamic behavior of MFC-GP plates governed by simply-supported boundary conditions, because the thermal-stress effect is obvious in this situation. Indeed, other boundary conditions have also been investigated to study the effect of transversal excitations on the dynamical stability of the structure, e.g. Ref. 10. However, the interesting phenomena of simply-supported MFC-GP plates indicate that the strongly coupled form can alter the nonlinear behavior of this structure. This offers important guidelines for the design of such composite structures in real engineering applications.

Acknowledgements

The authors gratefully acknowledge the support of the National Natural Science Foundation of China (NNSFC) (Grants No. 11772010, 11572006 and 11602210), the Funding Project for High Level Teachers' team construction in Beijing municipal colleges and Universities, and the Matching Grant from the Hong Kong Polytechnic University (4-BCDS).

Conflict of Interest

The authors declare that they have no conflict of interest with respect to the research, authorship, and/or publication of this article.

References

1. Novoselov, K. S.; Geim, A. K.; Morozov, S. V.; Jiang, D.; Zhang, Y.; Dubonos, S. V.; Grigorieva, I. V.; Firsov, A. A., Electric Field Effect in Atomically Thin Carbon Films. *Science* **2004,** *306* (5696), 666-669.
2. Novoselov, K., Nobel lecture: Graphene: Materials in the flatland. *Rev. Mod. Phys.* **2011,** *83* (3), 837.
3. Zhang, W.; Yang, J.; Hao, Y., Chaotic vibrations of an orthotropic FGM rectangular plate based on third-order shear deformation theory. *Nonlinear Dynamics* **2010,** *59* (4), 619-660.
4. Ansari, R.; Sahmani, S.; Arash, B., Nonlocal plate model for free vibrations of single-layered graphene sheets. *Phys. Lett. A* **2010,** *375* (1), 53-62.
5. Xu, K.; Wang, K.; Zhao, W.; Bao, W.; Liu, E.; Ren, Y.; Wang, M.; Fu, Y.; Zeng, J.; Li, Z., The positive piezoconductive effect in graphene. *Nature communications* **2015,** *6*, 8119.
6. Li, H.; Wang, X., Nonlinear frequency shift behavior of graphene–elastic–piezoelectric laminated films as a nano-mass detector. *International Journal of Solids and Structures* **2016,** *84*, 17-26.
7. Zhu, Z.; Wen, Y.; Sheng, H.; Xu, J., Nonlinear dynamic characteristics and bifurcation analysis of Al-doped graphene impacted by hydrogen atoms. *Int. J. Hydrogen Energy* **2017,** *42* (47), 28507-28514.
8. Shen, H.-S.; Lin, F.; Xiang, Y., Nonlinear vibration of functionally graded graphene-reinforced composite laminated beams resting on elastic foundations in thermal environments. *Nonlinear Dynamics* **2017,** *90* (2), 899-914.
9. Shen, H.-S.; Xiang, Y.; Fan, Y.; Hui, D., Nonlinear vibration of functionally graded graphene-reinforced composite laminated cylindrical panels resting on elastic foundations in thermal environments. *Composites Part B: Engineering* **2018,** *136*, 177-186.
10. Guo, X.; Jiang, P.; Zhang, W.; Yang, J.; Kitipornchai, S.; Sun, L., Nonlinear dynamic analysis of composite piezoelectric plates with graphene skin. *Composite Structures* **2018,** *206*, 839-852.
11. Wu, Z.; Chen, Y.; Bi, Q., Classification of nonlinear normal modes and their new constructive method. *ACTA MECHANICA SINICA-CHINESE EDITION-* **1996,** *28*, 298-307.
12. Li, X.; Chen, Y.; Wu, Z.; Chen, F., Bifurcation of nonlinear internal resonant normal modes of a class of multi-degree-of-freedom systems. *Mechanics Research Communications* **2002,** *29* (5), 299-306.
13. Lacarbonara, W.; Rega, G.; Nayfeh, A., Resonant non-linear normal modes. Part I: analytical treatment for structural one-dimensional systems. *International Journal of Non-Linear Mechanics* **2003,** *38* (6), 851-872.
14. Lacarbonara, W.; Rega, G., Resonant non-linear normal modes. Part II: activation/orthogonality conditions for shallow structural systems. *International Journal of Non-Linear Mechanics* **2003,** *38* (6), 873-887.
15. Sayed, M.; Mousa, A., Second-order approximation of angle-ply composite laminated thin plate under combined excitations. *Communications in Nonlinear Science and Numerical Simulation* **2012,** *17* (12), 5201-5216.
16. Jomehzadeh, E.; Afshar, M.; Galiotis, C.; Shi, X.; Pugno, N., Nonlinear softening and hardening nonlocal bending stiffness of an initially curved monolayer graphene. *International Journal of Non-Linear Mechanics* **2013,** *56*, 123-131.
17. Kwon, O. K.; Kim, K.-S.; Park, J.; Kang, J. W., Molecular dynamics modeling and simulations of graphene-nanoribbon-resonator-based nanobalance as yoctogram resolution detector. *Computational Materials Science* **2013,** *67*, 329-333.

18. Kwon, O. K.; Kim, H.-W.; Kang, J. W., Energy exchange between vibration modes of a graphene nanoflake oscillator: Molecular dynamics study. *Current Applied Physics* **2014,** *14* (3), 237-244.
19. Mousa, A.; Sayed, M.; Eldesoky, I.; Zhang, W., Nonlinear stability analysis of a composite laminated piezoelectric rectangular plate with multi-parametric and external excitations. *International Journal of Dynamics and Control* **2014,** *2* (4), 494-508
20. Mao, JJ.; Zhang, W., Linear and nonlinear free and forced vibrations of graphene reinforced piezoelectric composite plate under external voltage excitation. *Composite Structures* **2018**, *203*, 551-565.
21. S. K. Lai and L. H. Zhang, Thermal effect on vibration and buckling analysis of thin isotropic/orthotropic rectangular plates with crack defects, Eng. Struct. 177 (2018) 444–458.
22. Ji, H.; Sellan, D. P.; Pettes, M. T.; Kong, X.; Ji, J.; Shi, L.; Ruoff, R. S., Enhanced thermal conductivity of phase change materials with ultrathin-graphite foams for thermal energy storage. *Energy & Environmental Science* **2014,** *7* (3), 1185-1192.
23. Ma, W.; Liu, Y.; Yan, S.; Miao, T.; Shi, S.; Yang, M.; Zhang, X.; Gao, C., Systematic characterization of transport and thermoelectric properties of a macroscopic graphene fiber. *Nano Research* **2016,** *9* (11), 3536-3546.
24. Chen, H.; Ginzburg, V. V.; Yang, J.; Yang, Y.; Liu, W.; Huang, Y.; Du, L.; Chen, B., Thermal conductivity of polymer-based composites: Fundamentals and applications. *Prog. Polym. Sci.* **2016,** *59*, 41-85.
25. Burger, N.; Laachachi, A.; Ferriol, M.; Lutz, M.; Toniazzo, V.; Ruch, D., Review of thermal conductivity in composites: mechanisms, parameters and theory. *Prog. Polym. Sci.* **2016,** *61*, 1-28.
26. Y. Zhang, Q.-X. Pei, C.-M. Wang, C. Yang and Y.-W. Zhang, Interfacial thermal conductance and thermal rectification of hexagonal BCnN/graphene in-plane heterojunctions, J. Phys. Chem. C 122(39) (2018) 22783–22789.
27. Yang, B.; Yang, J.; Kitipornchai, S., Thermoelastic analysis of functionally graded graphene reinforced rectangular plates based on 3D elasticity. *Meccanica* **2017,** *52* (10), 2275-2292.
28. Phiri, J.; Johansson, L.-S.; Gane, P.; Maloney, T., A comparative study of mechanical, thermal and electrical properties of graphene-, graphene oxide-and reduced graphene oxide-doped microfibrillated cellulose nanocomposites. *Composites Part B: Engineering* **2018,** *147*, 104-113.
29. Shahrjerdi, A.; Yavari, S., Free vibration analysis of functionally graded graphene-reinforced nanocomposite beams with temperature-dependent properties. *Journal of the Brazilian Society of Mechanical Sciences and Engineering* **2018,** *40* (1), 25.
30. Vlassiouk, I.; Polizos, G.; Cooper, R.; Ivanov, I.; Keum, J. K.; Paulauskas, F.; Datskos, P.; Smirnov, S., Strong and electrically conductive graphene-based composite fibers and laminates. *ACS applied materials & interfaces* **2015,** *7* (20), 10702-10709.
31. Qin, L.; Li, L.; Wang, L.-k.; Sun, B., The study on the hydrostatic characteristic of 3-2 piezoelectric composite. *Journal of Functional Materials* **2007,** *38* (11), 1824.
32. Reddy, J. N., *Theory and analysis of elastic plates and shells*. CRC press: 2006.
33. Chia, C.-Y., *Nonlinear analysis of plates*. McGraw-Hill International Book Company: 1980.
34. Chen, J.; Zhang, W.; Guo, X.; Sun, M., Theoretical and experimental studies on nonlinear oscillations of symmetric cross-ply composite laminated plates. *Nonlinear Dynamics* **2013,** *73* (3), 1697-1714.

35. C. S. Wu, Y. L. Liu, Y. C. Chiu and Y. S. Chiu, Thermal stability of epoxy resins containing °ame retardant components: An evaluation with thermogravimetric analysis, Polym. Degrad. Stab. 78(1) (2002) 41–48.

Appendix

$$M_i = \frac{a_g g_{3gi} \bar{s}_i + (1-a_g)\bar{g}_{3pmi} s_i}{(1-a_g)s_i + a_g \bar{s}_i} \qquad (i=1,2) \tag{A1}$$

$$N_i = a_g \beta_{33g}^T + (1-a_g)\bar{\beta}_{33pm}^T + \frac{a_g (g_{3gi})^2}{s_i} + \frac{(1-a_g)(\bar{g}_{3pmi})^2}{\bar{s}_i} \tag{A2}$$

$$-\left[\frac{a_g g_{3gi}}{s_i} + \frac{(1-a_g)\bar{g}_{3pmi}}{\bar{s}_i}\right]\left[\frac{a_g g_{3gi}\bar{s}_i + (1-a_g)\bar{g}_{3pmi} s_i}{a_g \bar{s}_i + (1-a_g)s_i}\right] \qquad (i=1,2)$$

$$s_i = s_{11g}^E + s_{12g}^E - \frac{d_{3gi}^2}{\varepsilon_{33g}^T} \qquad (i=1,2) \tag{A3}$$

$$\bar{s}_i = \left[a_p (s_{11}^{Ep} + s_{12}^{Ep}) + (1-a_p)(s_{11}^{Em} + s_{12}^{Em}) - s_3 - s_{4i}\right] \qquad (i=1,2) \tag{A4}$$

$$s_3 = \frac{2a_p(1-a_p)(s_{13}^{Ep} - s_{12}^{Em})^2}{s(a)} \tag{A5}$$

$$s_{4i} = \frac{2a_p^2\left[d_{3pi} - \dfrac{(1-a_p)d_{33p}(s_{13}^{Ep} - s_{12}^{Em})}{s(a)}\right]^2}{\left[a_p \varepsilon_{33}^{Tp} - \dfrac{a_p(1-a_p)d_{33p}^2}{s(a)} + (1-a_p)\varepsilon_{11}^{Em}\right]} \qquad (i=1,2) \tag{A6}$$

$$g_{3gi} = \frac{d_{3gi}}{\varepsilon_{33}^T} \qquad (i=1,2) \tag{A7}$$

$$\bar{g}_{3pmi} = \frac{a_p\left[d_{3pi} - \dfrac{(1-a_p)d_{33p}(s_{13}^{Ep} - s_{12}^{Em})}{s(a)}\right]}{\left[a_p \varepsilon_{33}^{Tp} - \dfrac{a_p(1-a_p)d_{33p}^2}{s(a)} + (1-a_p)\varepsilon_{11}^{Tm}\right]} \qquad (i=1,2) \tag{A8}$$

$$\beta_{33g}^T = \frac{1}{\varepsilon_{33}^T} \tag{A9}$$

$$\bar{\beta}_{33pm}^T = \frac{1}{\left[a_p \varepsilon_{33}^{Tp} - \dfrac{a_p(1-a_p)d_{33p}^2}{s(a)} + (1-a_p)\varepsilon_{11}^{Tm}\right]} \tag{A10}$$

$$s(a) = a_p s_{11}^{Em} + (1-a_p)s_{33}^{Ep} \tag{A11}$$

The values of the MFC-GP material properties can be referred to Table 1.

Captions of Figures

Fig. 1 Schematic of a composite plate with graphene skins.

Fig. 2 Schematic of a MFC-GP composite plate under an external force.

Fig. 3 Frequency-response curves of the first-order mode under different GP volume fractions.

Fig. 4 Frequency-response curves of the second-order mode under different GP volume fractions.

Fig. 5 Frequency-response curves of the second-order mode under different temperature.

Fig. 6 Frequency-response curves of the second-order mode under different external forces.

Fig. 7 Frequency-response curves of the first-order mode under different voltages.

Fig. 8 Frequency-response curves of the first-order mode under different GP volume fractions.

Fig. 9 Frequency-response curves of the second-order mode under different GP volume fractions.

Fig. 10 Frequency-response curves of the first-order mode under different temperature.

Fig. 11 Frequency-response curves of the second-order mode under different external excitations.

Fig. 12 Frequency-response curves of the first-order mode under different voltages.

Fig. 13 Frequency-response curves of the first-order mode under different GP volume fractions.

Fig. 14 Frequency-response curves of the second-order mode under different GP volume fractions.

Fig. 15 Frequency-response curves of the first-order mode under different temperature.

Fig. 16 Frequency-response curves of the second-order mode under different temperature.

Fig. 17 Frequency-response curves of the first-order mode under different external excitations.

Fig. 18 Frequency-response curves of the second-order mode under different external excitations.

Fig. 19 Frequency-response curves of the first-order mode under different voltages.

Fig. 20 Frequency-response curves of the second-order mode under different voltages.

Captions of Tables

Table 1 Properties of the MFC-GP material.

Table 2 Natural frequencies for simply-supported MFC-GP rectangular plates.

Table 3 Effects of different parameters on two vibration modes.

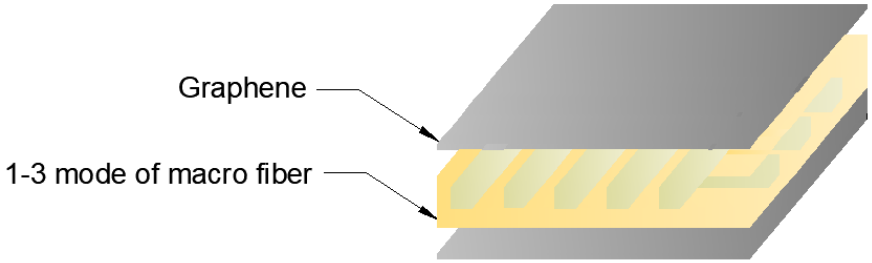

Fig. 1 Schematic of a composite plate with graphene skins.

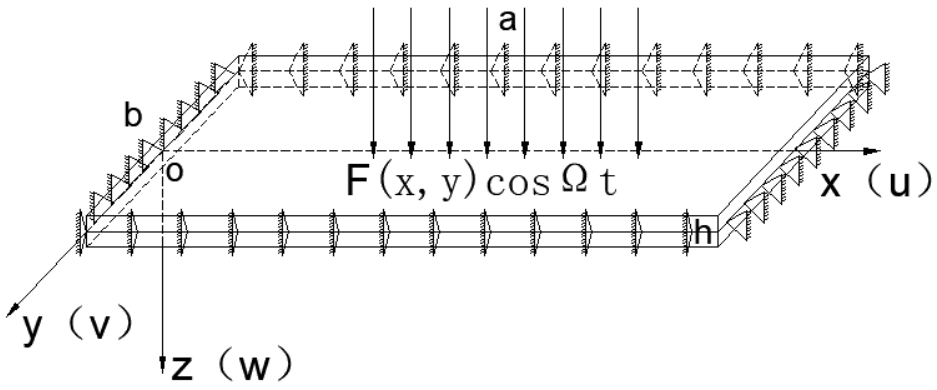

Fig. 2 Schematic of a MFC-GP composite plate under an external force.

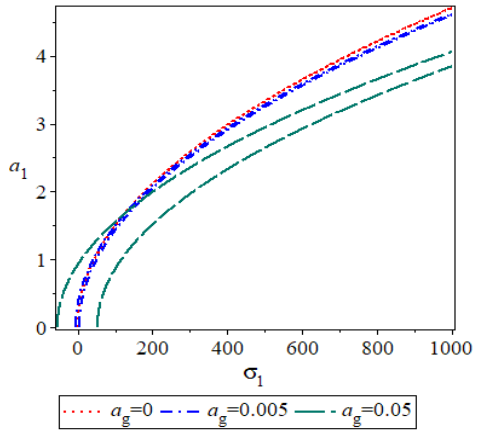

Fig.3 Frequency-response curves of the first-order mode under different GP volume fractions.

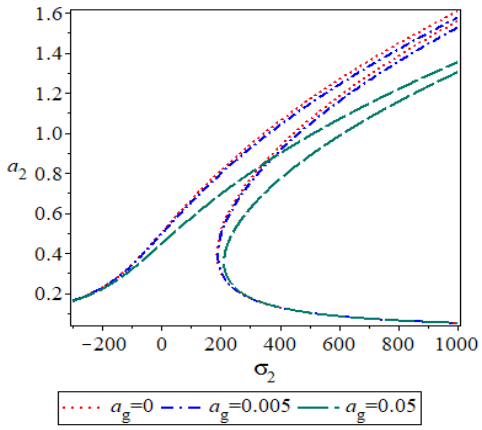

Fig.4 Frequency-response curves of the second-order mode under different GP volume fractions.

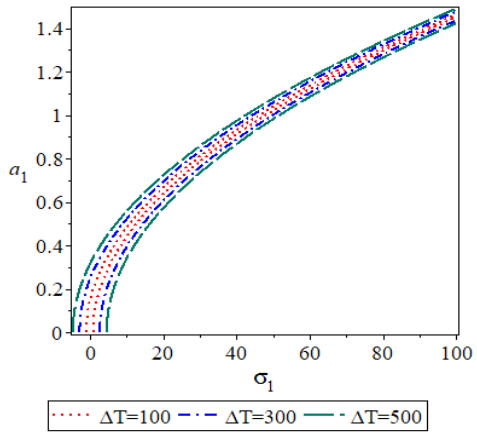

Fig.5 Frequency-response curves of the second-order mode under different temperature.

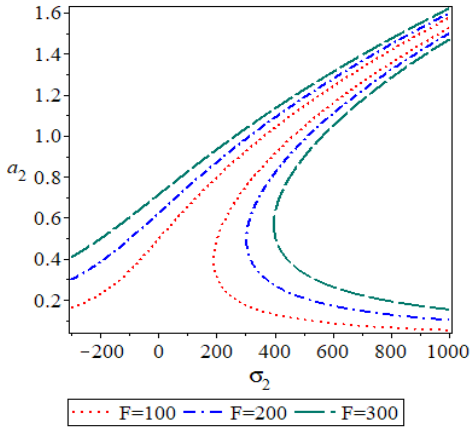

Fig.6 Frequency-response curves of the second-order mode under different external forces.

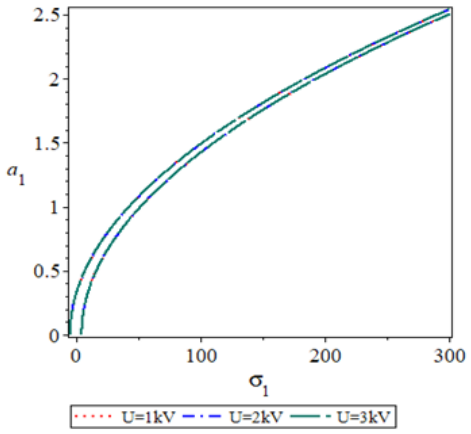

Fig.7 Frequency-response curves of the first-order mode under different voltages.

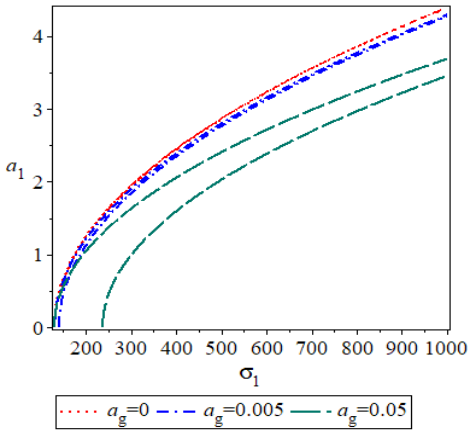

Fig.8 Frequency-response curves of the first-order mode under different GP volume fractions.

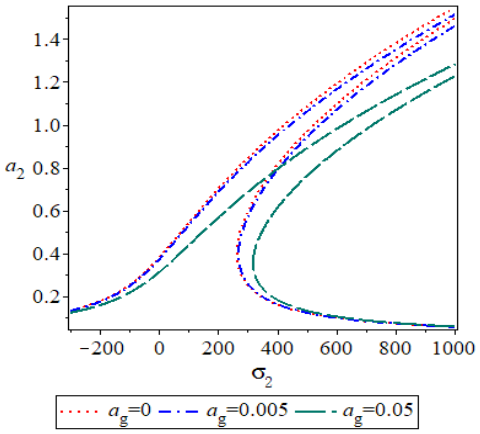

Fig.9 Frequency-response curves of the second-order mode under different GP volume fractions.

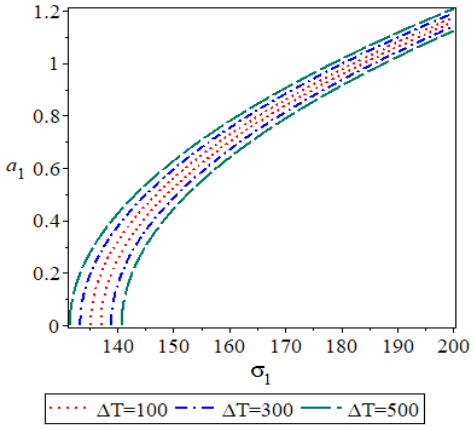

Fig.10 Frequency-response curves of the first-order mode under different temperature.

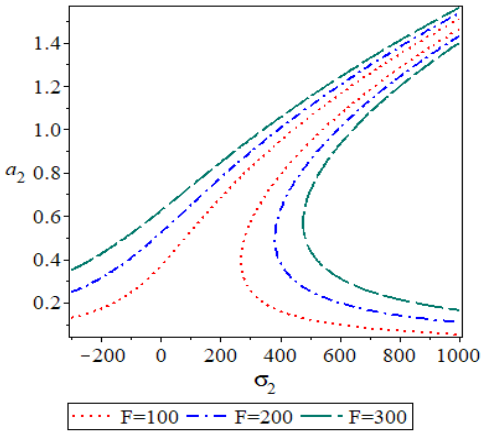

Fig.11 Frequency-response curves of the second-order mode under different external excitations.

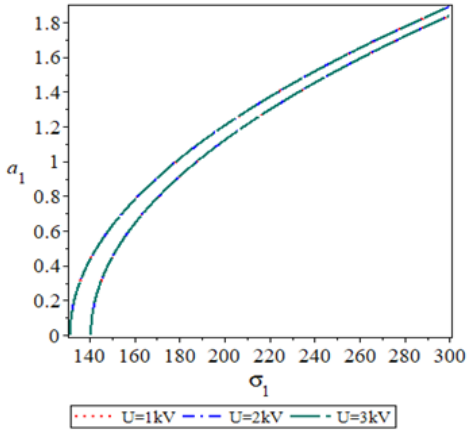

Fig.12 Frequency-response curves of the first-order mode under different voltages.

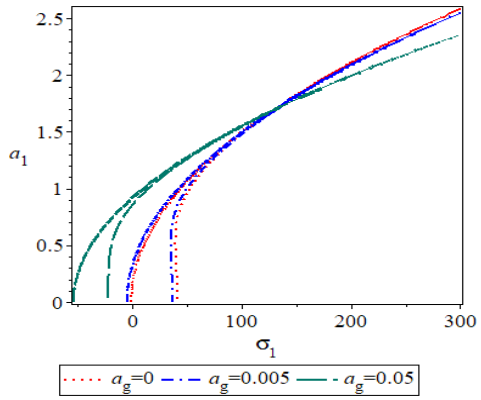

Fig.13 Frequency-response curves of the first-order mode under different GP volume fractions.

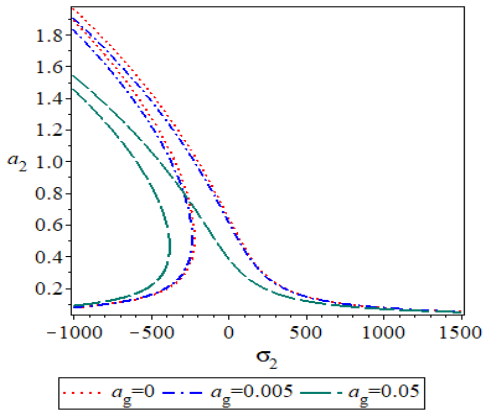

Fig.14 Frequency-response curves of the second-order mode under different GP volume fractions.

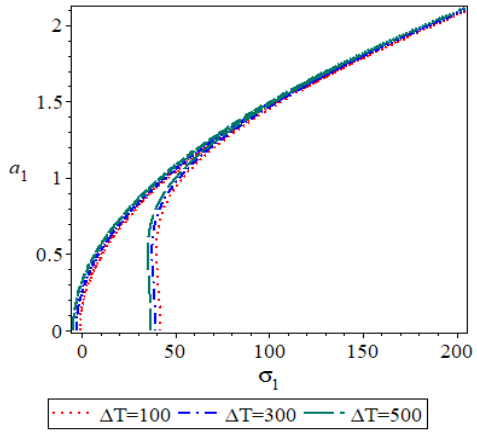

Fig.15 Frequency-response curves of the first-order mode under different temperature.

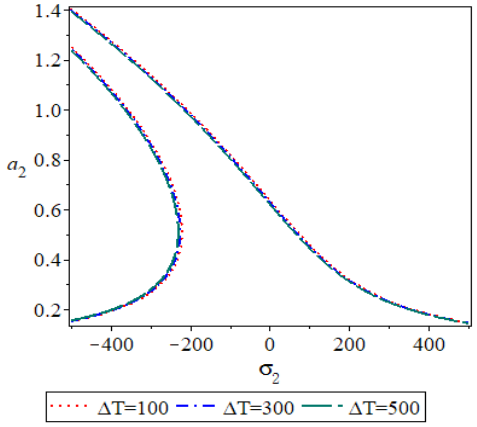

Fig.16 Frequency-response curves of the second-order mode under different temperature.

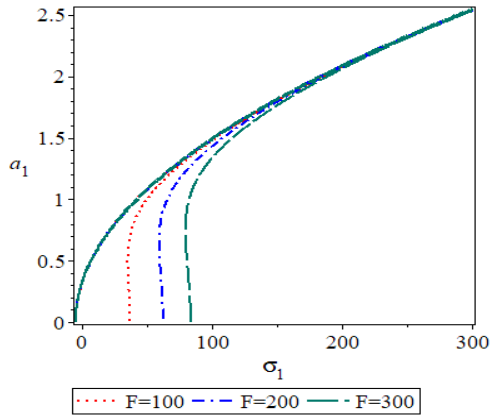

Fig.17 Frequency-response curves of the first-order mode under different external excitations.

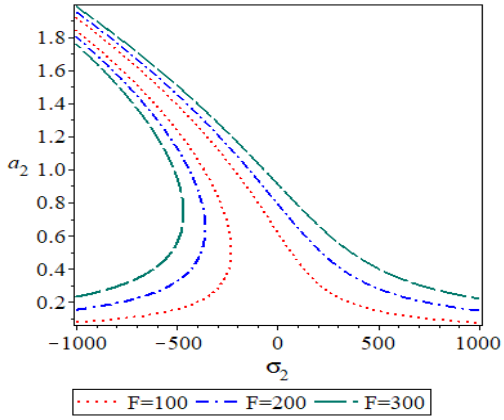

Fig.18 Frequency-response curves of the second-order mode under different external

excitations.

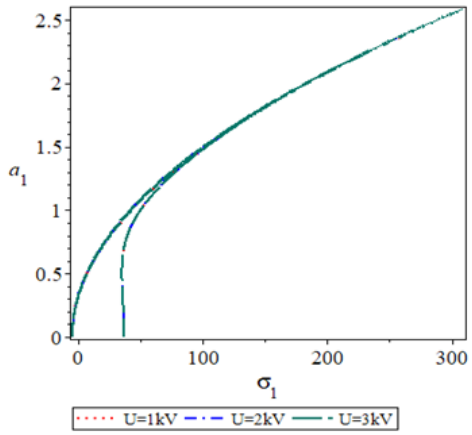

Fig.19 Frequency-response curves of the first-order mode under different voltages.

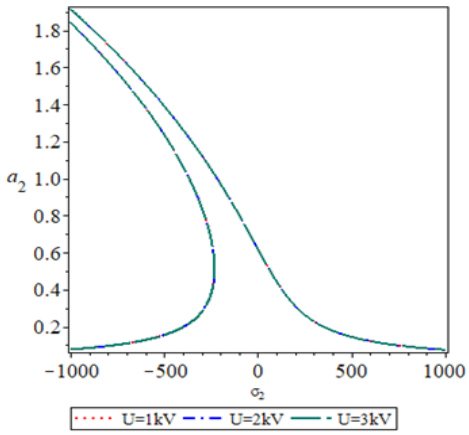

Fig.20 Frequency-response curves of the second-order mode under different voltages.

Table 1 Properties of the MFC-GP material.

Material properties	Epoxy	GPL	MFC
Young's modulus (GPa)	3.0	1010	210
Density (kg m^{-3})	1200	1062.5	7450
Poisson's ratio	0.34	0.186	0.3
Dielectric constant(C/m^2)	$\varepsilon_{11} = 10$	$\varepsilon_{33} = 726$	$\varepsilon_{33} = 350$
Piezo-electrical-strain coefficient (pC/N)	0	$d_{31} = -250$ $d_{32} = 200$ $d_{33} = 600$	$d_{31} = -250$ $d_{32} = 300$ $d_{33} = 1400$
Flexibility coefficient (10^{-12} m^2/N)	$s_{11} = 185.6$ $s_{12} = -360.3$	$s_{11} = 0.8$ $s_{12} = -3.6$	$s_{11} = 3.5$ $s_{12} = -8.3$

Table 2 Natural frequencies for simply-supported MFC-GP rectangular plates.

Modes / Natural frequencies / Volume fraction of GP	$m=1$ $n=1$	$m=1$ $n=2$	$m=2$ $n=1$	$m=2$ $n=2$	$m=1$ $n=3$	$m=3$ $n=1$	$m=2$ $n=3$	$m=3$ $n=2$
0	1.96	3.36	2.84	3.97	4.85	3.79	5.32	4.73
0.005	**1.97**	3.46	3.02	4.20	4.95	**3.84**	5.62	4.88
0.05	2.03	4.25	4.18	5.72	5.78	4.15	7.62	6.04

Table 3 Effects of different parameters on two vibration modes.

Mode \ Parameter		Volume fraction of graphene (a_g)↑	Voltage (U)↑	Temperature Difference (ΔT)↑	External Excitation (F)↑
Uncoupled case of two modes	First-order mode	Hardening spring characteristic ↑	Not obvious	Resonance region ↑	—
	Second-order mode	Ditto	—	—	Resonance region ↑
Weakly coupled case of two modes	First-order mode	Hardening spring characteristic↑, Resonant frequency↑	Not obvious	Resonance region↑, Resonant frequency↑	—
	Second-order mode	Ditto	—	—	Resonance region↑, Resonant frequency↑
Strongly coupled case of two modes	First-order mode	Hardening spring characteristic↑	Not obvious	Resonance frequency ↓	Resonance region↑
	Second-order mode	Soft spring characteristic↑	Not obvious	Resonance frequency ↓	Resonance region↑